

Modeling of dual frequency capacitively coupled plasma sources utilizing a full-wave Maxwell solver: II. Scaling with pressure, power and electronegativity

This article has been downloaded from IOPscience. Please scroll down to see the full text article.

2010 Plasma Sources Sci. Technol. 19 055012

(<http://iopscience.iop.org/0963-0252/19/5/055012>)

View [the table of contents for this issue](#), or go to the [journal homepage](#) for more

Download details:

IP Address: 141.213.8.59

The article was downloaded on 10/10/2010 at 16:30

Please note that [terms and conditions apply](#).

Modeling of dual frequency capacitively coupled plasma sources utilizing a full-wave Maxwell solver: II. Scaling with pressure, power and electronegativity

Yang Yang^{1,3} and Mark J Kushner^{2,4}

¹ Iowa State University, Department of Electrical and Computer Engineering, Ames, IA 50011, USA

² University of Michigan, Department of Electrical Engineering and Computer Science, 1301 Beal Avenue, Ann Arbor, MI 48109, USA

E-mail: yang_yang@amat.com and mjkush@umich.edu

Received 15 February 2010, in final form 29 June 2010

Published 20 September 2010

Online at stacks.iop.org/PSST/19/055012

Abstract

The trend in dielectric etching in microelectronics fabrication with capacitively coupled plasmas is the use of multiple frequencies where a high frequency (HF, tens to hundreds of MHz) dominates ionization and a low frequency (LF, a few to tens MHz) is used to control ion energy distributions to the wafer. Process parameters, such as pressure, gas mixture and LF and HF power deposition, are important to determining the uniformity of the plasma and properties of ions incident on the wafer. In this paper, we report on a computational investigation of the consequences of these parameters on uniformity and ion energy distributions to the wafer in a dual frequency capacitively coupled plasma reactor sustained in Ar/CF₄ gas mixtures. Due to the coupling of finite wavelength, electromagnetic skin, electrostatic edge and electronegative effects, there are no simple scaling laws for plasma uniformity. The plasma uniformity is ultimately a function of conductivity and energy relaxation distance of electrons accelerated by electric fields in and near the sheath. There is a strong second-order effect on uniformity due to feedback from the electron energy distributions (EEDs) to ionization sources. The trends from our parametric study are correlated with the spatial variation of the HF electric field, to the total power deposition and to the spatial variation of EEDs and ionization sources.

(Some figures in this article are in colour only in the electronic version)

1. Introduction

An advanced feature of capacitively coupled plasma (CCP) tools currently under development and being utilized for plasma etching of microelectronics devices is the application of multiple power sources at different frequencies [1–3]. Typically in a dual frequency capacitively coupled plasma (DF-CCP) reactor, power is applied at a low frequency (LF) to the bottom electrode (a few MHz to 10 MHz) holding the

wafer; and high frequency (HF) power is applied to the upper electrode (tens of MHz to hundreds of MHz) often also serving as the gas injecting shower head. (Some variations of DF-CCPs apply both frequencies to the lower electrode [4]). The goal of using very HF power sources (>100 MHz) is to better control the resulting electron energy distributions (EEDs) in the plasma and so better control the cracking patterns of the feedstock gases by electron impact. If achieved, this control over fragmentation patterns of the gases will produce finer control over the reactant fluxes to the substrate which in turn more reliably produce the etch.

As the plasma reduced wavelength of the radio frequency (rf) power applied to the reactor approaches the size of the

³ Present Address: Applied Materials, Inc., 974 E. Arques Ave., Sunnyvale, CA 94085, USA.

⁴ Author to whom any correspondence should be addressed.

reactor, finite wavelength effects and skin effects become increasingly more important in determining plasma uniformity [5, 6]. In essence, instead of the electric potential appearing simultaneously across the face of the electrode (a purely electrostatic (ES) condition), the electric potential is carried by a wave which propagates from the cable feed to the reactor at the back of the electrode, around the electrodes and into the plasma. The waves then appear to propagate inward from the edges of the electrodes which provides the possibility of constructively interfering at the center of the electrode. For sufficiently short wavelengths, the electric field can be magnified at the center of the reactor by this constructive interference compared with the edges. The electric fields are additionally electrostatically enhanced at the edge of the electrodes, where a finite skin depth for penetration of the electromagnetic (EM) wave into the bulk of the plasma may also limit power deposition [6].

To investigate these issues, we developed a two-dimensional hybrid simulation for a DF-CCP reactor with which we addressed plasmas sustained in Ar and Ar/CF₄. The model is described in part I of our investigation [7]. The consequences of varying the HF on plasma properties were analyzed in part I by correlating the spatial variation of the phase, magnitude and wavelength of the HF electric field to the spatial variation of the EEDs and ionization sources. In this paper, the effects of pressure, HF and LF power deposition (P_{HF} , P_{LF}), and gas mixtures on plasma properties are examined with an emphasis on the effects on plasma uniformity. We found that when increasing pressure from 25 to 150 mTorr in Ar/CF₄ = 90/10 mixtures, the electron density transitions from middle high (meaning the maximum is at a middle radius of the wafer) to center high (meaning the maximum is at the center of the reactor) as the energy relaxation distance decreases and more power deposition occurs along the HF sheath. The radial profile of electron impact ionization sources begins to mirror that of the electric field in the HF sheath at higher pressures. The HF field is center peaked due to the constructive interference of counter-propagating waves, a phenomenon we term the finite wavelength effect [7]. At 50 mTorr, increasing P_{HF} (from 300 W to 1000 W) or P_{LF} (from 300 W to 1500 W) decreases the uniformity of the plasma in Ar/CF₄ mixtures due to dissociative attachment processes and non-uniform power deposition along the HF sheath. With increasing CF₄ fraction, the decreasing plasma conductivity increases the effective wavelength of the incident wave in the plasma. The power deposition then transitions from being dominated by EM effects to ES effects, and the maximum electron density shifts toward being edge high (meaning the maximum electron density is near the edge of electrode). The uniformity of the plasma is improved for CF₄ fractions larger than 0.2, which translates to improve radial uniformity of the ion fluxes and ion energy and angular distributions (IEADs) incident on the wafer.

The model is briefly described in section 2 and the results of our parametric study are discussed in section 3. Concluding remarks are in section 4.

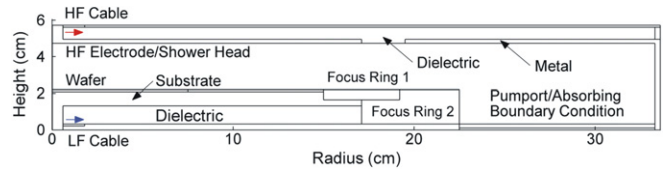


Figure 1. Schematic of the DF-CCP reactor. The wafer sits on a substrate powered at LF and surrounded by dielectric focus rings. The showerhead is powered at HF and is also surrounded by a dielectric. The HF and LF fields are launched where the cables are connected to the reactor.

2. Description of the model

The model used in this investigation is the two-dimensional Hybrid Plasma Equipment Model (HPEM) which incorporates a full-wave solution of Maxwell's equations. The model is the same as that described in part I [7] and [8].

Briefly, continuity, momentum and energy equations for neutrals and ions; continuity equations for electrons and Maxwell's equations are integrated in time over many hundred rf cycles to obtain a periodic steady state. The resulting electric fields and ion fluxes to surfaces are periodically transferred to the electron Monte Carlo simulation (EMCS) module where the energy transport of bulk electrons and secondary electrons emitted from surfaces is addressed. Electron transport coefficients, temperatures, impact source functions and sources of secondary electron current obtained from the EMCS are returned to the fluid model. The process is iterated to convergence. During the last iteration, the converged electric fields and source functions for ions and neutrals are recorded as a function of position and phase in the rf cycle. With these values, the energy and angular distributions of ions and neutrals incident on the substrate are obtained using a Monte Carlo simulation. Powers are separately specified for the LF and HF sources, and the applied voltages are adjusted to deliver those powers. The powers are computed from $P = (1/\Delta t) \int VI \cdot dt$, where V and I are the voltage and total current at the surface of the electrode, and the integration is over Δt , the LF period.

Solving the full set of Maxwell's equations is computationally challenging but does enable us to address the inductive effects that result from wave penetration at HF into plasmas and finite wavelength effects, in addition to the ES effects. In our model, we separately solve for the EM field (from rf sources) and the ES field (from charges), and sum the fields for plasma transport. The solution was implemented in the time domain so that coupling between frequencies could be explicitly addressed as well as intra-rf period feedback between plasma transport and the EM wave. The reaction mechanisms for the Ar and Ar/CF₄ mixtures used in this study are discussed in [9].

3. Plasma properties in DF-CCP reactors: pressure, power and gas chemistry

The model reactor used in this study is schematically shown in figure 1. The base case uses a metal substrate powered at the LF (10 MHz) through a blocking capacitor. A conductive

Si wafer ($\sigma = 0.01 \Omega^{-1} \text{cm}^{-1}$), 30 cm in diameter, sits in electrical contact with the substrate which is surrounded by a Si ring (focus ring 1, $\varepsilon/\varepsilon_0 = 12.5$, $\sigma = 10^{-6} \Omega^{-1} \text{cm}^{-1}$) and a dielectric focus ring (focus ring 2, $\varepsilon/\varepsilon_0 = 8.5$, $\sigma = 10^{-8} \Omega^{-1} \text{cm}^{-1}$). The substrate is also encased in a dielectric having $\varepsilon/\varepsilon_0 = 4.0$. Gas is injected through a shower head 34 cm in diameter that also serves as the HF electrode. The HF electrode is surrounded by a dielectric having $\varepsilon/\varepsilon_0 = 4.0$. All other surfaces in the reactor are grounded metal including the annular pump port.

3.1. Pressure

Increasing pressure increases electron–neutral collision frequencies, reduces the mean free path for energy relaxation and reduces diffusion losses, thereby increasing the plasma density for a constant power deposition. This increase in plasma density has been experimentally observed over a wide range of operating conditions in HF CCP discharges [10]. An increase in the electron density above the increase in pressure, that is an increasing conductivity, emphasizes skin depth effects by shortening the absorption length, thereby increasing the relative power deposition near the edges of the electrodes where the EM field enters the plasma. The energy relaxation distance also decreases with increasing pressure, thereby localizing power deposition that is produced by ES field enhancement at the edges of the electrodes. So transitioning to an edge-high distribution of plasma is expected with increasing pressure. Volynets *et al* performed diagnostics in a single frequency CCP reactor driven at 100 MHz in pure argon and argon/fluorocarbon gas mixtures [11]. With increasing pressure and holding power constant at 750 W, they found that the spatial distribution of the plasma transitioned from center high at 10 mTorr to center-and-edge high at 80 mTorr (with a higher peak at the edge).

In pure Ar discharges, our computational results qualitatively agree with the experiments of [11]. To match the conditions in [11], a 100 MHz rf source was applied on the upper electrode delivering 750 W to sustain a pure Ar discharge (no LF power). At 100 MHz, the electric field in the sheath is center peaked due to the constructive interference resulting from the finite wavelength effect [7]. The electron density as a function of radius is shown in figure 2 at the middle of the electrode gap for 10, 50 and 80 mTorr. With increasing pressure, the electron density transitions from center high at 10 and 50 mTorr to edge high at 80 mTorr. This center high to edge-high transition results from skin effects associated with the evanescent wave propagating into the bulk plasma at the edge of the electrode which dominates over the surface wave propagating along the HF sheath.

The behavior of HF discharges as a function of pressure depends on the gas mixture—there are systematic differences between electropositive and electronegative discharges. To investigate the consequences of pressure on plasma uniformity in electronegative gas mixtures, the LF and HF were held constant at 10 MHz and 150 MHz, respectively, each delivering 300 W. The gas mixture was $\text{Ar}/\text{CF}_4 = 90/10$. The electron density ($[e]$) is shown in figure 3 while varying pressure from 25

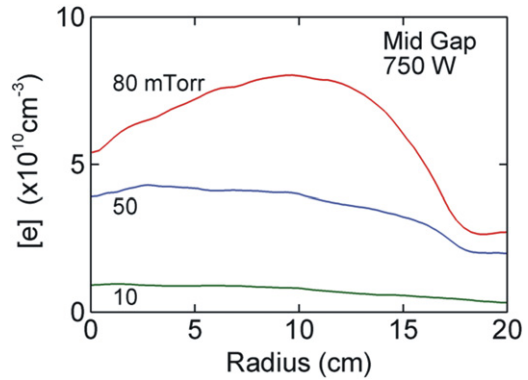


Figure 2. Time averaged electron density as a function of radius at mid-gap with a single frequency excitation (100 MHz from the upper electrode) in pure Ar discharges.

to 150 mTorr. The electron density has been averaged over the longer LF cycle. (The plasma is fairly well confined between the electrodes and so only the region of the reactor directly above the substrate is shown in this and the following figures.) With increasing pressure, the electron density moderately increases from a maximum of $9.8 \times 10^{10} \text{cm}^{-3}$ at 25 mTorr to $1.4 \times 10^{11} \text{cm}^{-3}$ at 150 mTorr. Exceeding 50 mTorr, the maximum in electron density shifts toward the center of the reactor and toward the HF electrode. This inward shift with increasing pressure differs from what was observed in Ar discharges (an outward shift) and largely results from an interplay between energy relaxation distances and attachment rates.

The magnitude of the HF electric field (first harmonic amplitude, E_m) in the HF sheath is shown in figure 4(a) as a function of radius for pressures from 25 to 150 mTorr. The electric fields are normalized by their values at $r = 0$ to emphasize their radial variations. From 25 to 150 mTorr, the radial profile of the E_m largely remains the same as the electron density is only increased by a factor of 1.4. Given the increase in electron collision frequency with increasing pressure, the small change in electron density is not sufficient to produce dramatic changes in the plasma-shortened wavelength. As such, the finite wavelength effect alone is not responsible for the transition from middle high to center high electron densities.

Concurrent to local changes in electron density with increasing pressure, the electron–neutral collision frequencies also increase. So the plasma conductivity, and consequently the skin depth, are not strictly linear functions of pressure, as shown in figure 4(b). The magnitude of the radial HF field (first harmonic amplitude, E_{mr}), a measure of the inductive field, as a function of radius in the middle of the electrode gap is shown in figure 4(c) for pressures from 25 to 150 mTorr. Exceeding 75 mTorr, E_{mr} decreases with pressure at small radii, an indication of the plasma overall being less conductive. Near the edge of the HF electrode ($r = 17 \text{cm}$), E_{mr} does not change systematically with pressure—the peak values of E_{mr} at 100 mTorr and 150 mTorr are less than that at 25 mTorr. As such, the inductive heating from the E_{mr} and skin effects are not particularly enhanced with increasing pressure under our operating conditions. This differs from the pure argon case.

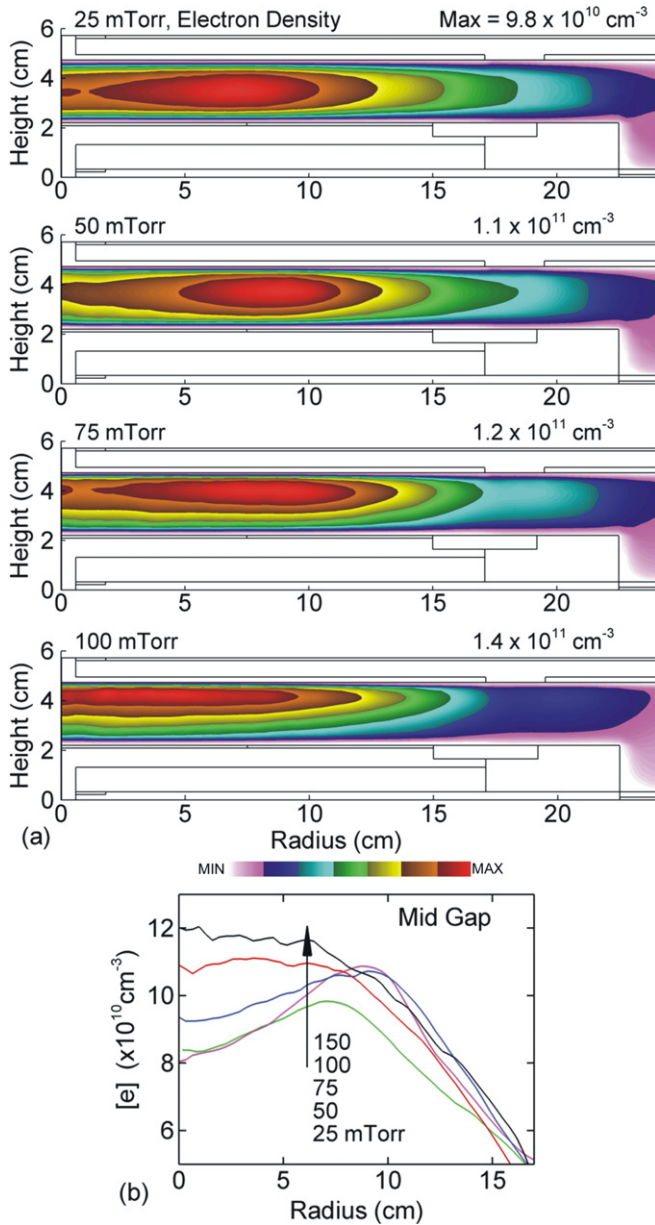


Figure 3. Time averaged electron density ($[e]$) for increasing pressure ($\text{Ar}/\text{CF}_4 = 90/10, P_{\text{HF}} = P_{\text{LF}} = 300 \text{ W}$, $\text{HF} = 150 \text{ MHz}$, $\text{LF} = 10 \text{ MHz}$). (a) Electron density for pressures of 25, 50, 75 and 100 mTorr, (b) radial $[e]$ profile at mid-gap. The maximum value or range of values in each frame is noted. The electron density is on a linear scale. The maximum of the electron density shifts toward the center of the reactor and toward the HF electrode with increasing pressure. The finite wavelength effect is not responsible for this shift.

The consequences of the shortening of the energy relaxation distance with increasing pressure on the spatial distribution of EEDs are partly shown in figure 5, where EEDs at different distances from the HF electrode are plotted at $r = 5 \text{ cm}$ for 25 and 150 mTorr. At 25 mTorr, the EEDs in the bulk plasma ($d = 1.7\text{--}0.3 \text{ cm}$ where d is the distance from the HF electrode) are largely indistinguishable due to the long energy relaxation distance and uniform Ohmic heating in the bulk plasma. The energy relaxation distance can be estimated by $\lambda_\varepsilon \approx (\lambda_m \lambda_{\text{in}}/3)^{1/2}$, where λ_m is the total mean free path for

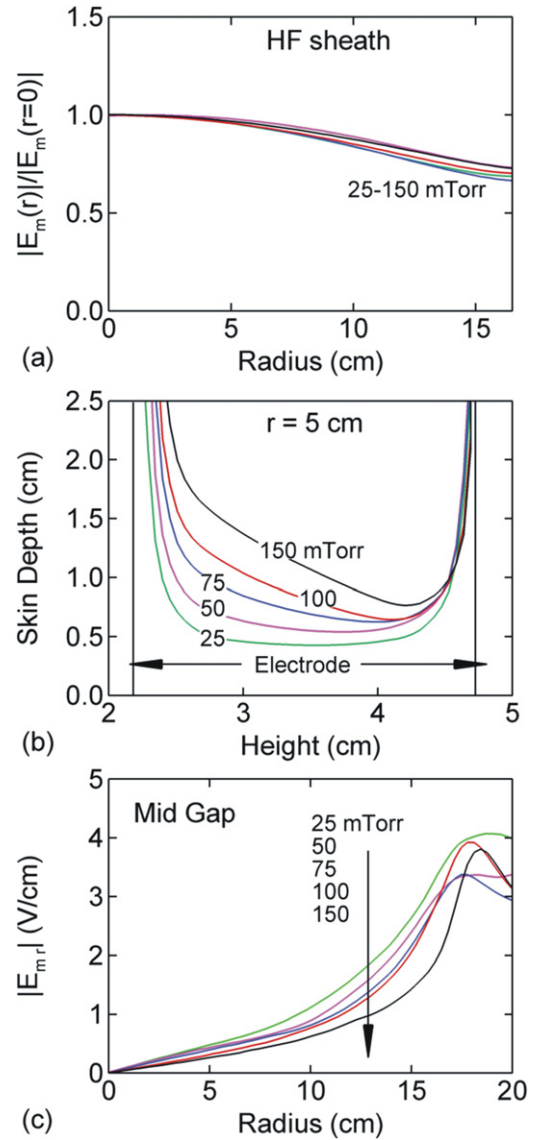


Figure 4. EM properties for pressures of 25, 50, 75, 100 and 150 mTorr ($\text{Ar}/\text{CF}_4 = 90/10, P_{\text{HF}} = P_{\text{LF}} = 300 \text{ W}$, $\text{HF} = 150 \text{ MHz}$, $\text{LF} = 10 \text{ MHz}$). (a) Magnitude of the HF electric field (first harmonic amplitude, E_m) along the HF sheath (normalized by the magnitude of the field at the center of the reactor), (b) skin depth as a function of height at $r = 5 \text{ cm}$ and (c) magnitude of the radial HF electric field (first harmonic amplitude, $|E_{m,r}|$). The skin depth and the maximum of $|E_{m,r}|$ are not linear functions of pressure due to the nonlinear changes in the plasma conductivity.

momentum transfer and λ_{in} is the mean free path accounting for all collisional energy loss processes [12]. λ_ε decreases from 2.1 to 0.36 cm from 25 to 150 mTorr. The tails of EEDs near the HF sheath ($d = 0.1$ and 0.2 cm) are lifted due to the stochastic sheath heating that dominates at 150 MHz, effects that are captured by the Monte Carlo simulation used in the model. At 150 mTorr, there is a systematic depression of the EEDs from the HF electrode into the bulk plasma due to the shortening of the energy relaxation distance. At the lower pressure, the tail remains high to mid-gap.

The shortening of the energy relaxation distance with increasing pressure also results in increasing power deposition

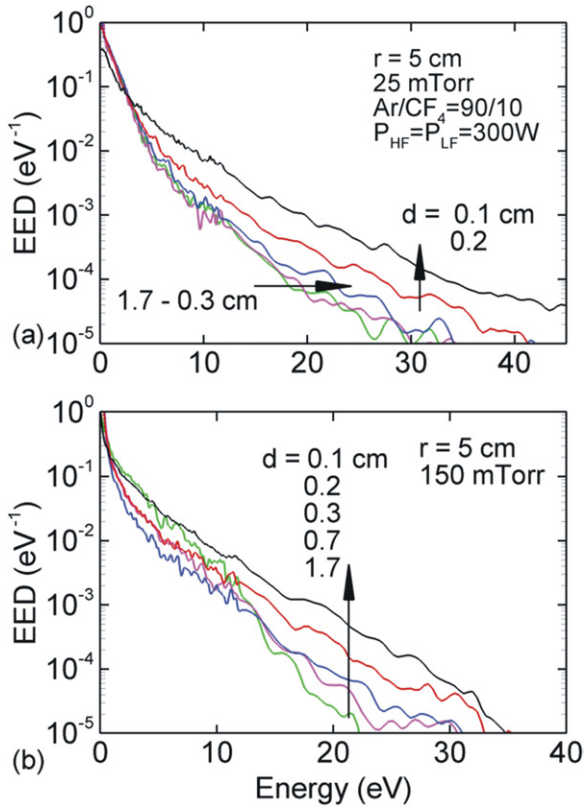


Figure 5. EEDs at different axial locations at $r = 5$ cm ($\text{Ar}/\text{CF}_4 = 90/10$, $P_{\text{HF}} = P_{\text{LF}} = 300$ W, HF = 150 MHz, LF = 10 MHz). (a) 25 mTorr, (b) 150 mTorr. The distances d from the HF electrode are noted in each frame. At 150 mTorr, the electron energies are systematically degraded from the HF electrode into the bulk plasma due to the shortening of the energy relaxation distance.

along the HF sheath, as shown in figures 6(a) and (b). The total power deposition is obtained by an average over the LF cycle of the instantaneous power, $P_{\text{tot}} = (1/\Delta t) \int \vec{E} \cdot \vec{J} dt$, where Δt is the LF period. Note that the power deposition shown here is where power flows into the electrons and not where power flows out of the electrons into the gas. The axial location where power flows into the electrons does not significantly vary as a function of pressure since that quantity depends largely on sheath thickness, which is a weak function of pressure. The electron impact source functions are a clearer indication of where energy flows out of the electrons into the gas. With the decrease in mean free path, the bulk electron impact source function (S_e) becomes increasingly peaked in the HF sheath with increasing pressure, as shown in figure 6(c). In turn, in the radial direction, S_e increasingly mirrors the electric field in the HF sheath (figure 6(d)), which is center peaked due to the finite wavelength effect. The close correlation of S_e with power deposition and the decrease in energy relaxation distance is ultimately responsible for the shift of the peak electron density toward the center of the reactor with increasing pressure. With increasing pressure, attachment progressively dominates over ionization processes in the bulk plasma adjacent to the HF sheath and so net electron losses result, as shown in figure 6(c). Further into the bulk plasma, the attachment losses decrease as the epi-thermal portion of the EED that overlaps

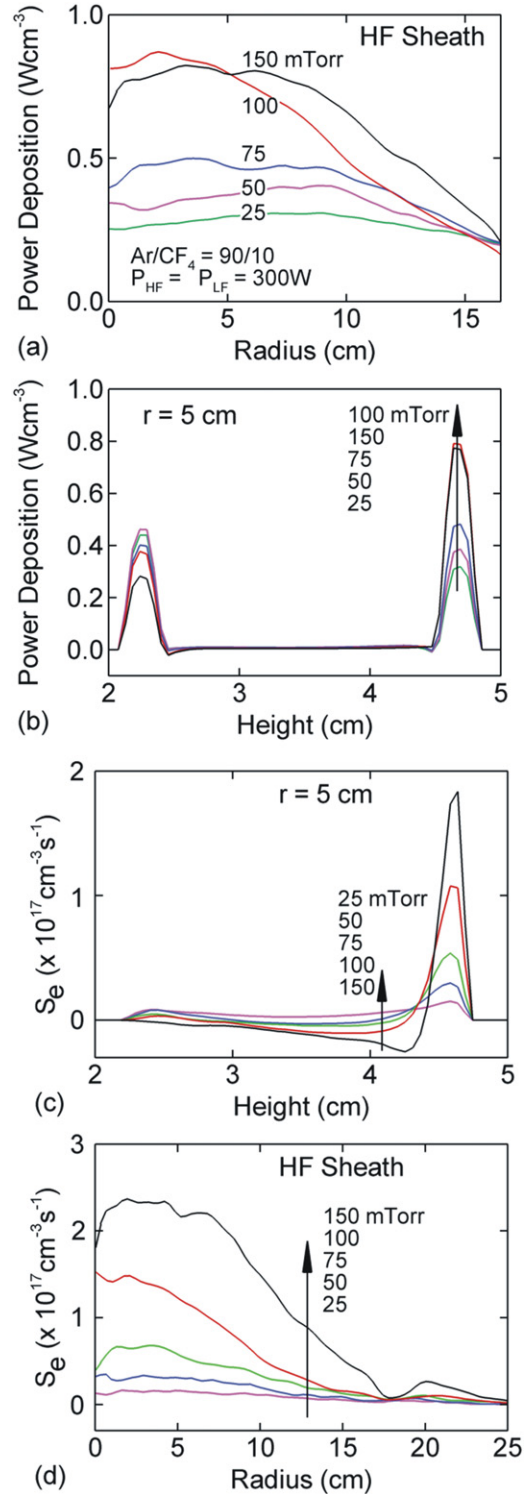


Figure 6. Time averaged total power deposition ($P_{\text{tot}} = (1/\Delta t) \times \int \vec{E} \cdot \vec{J} \Delta t$) and bulk electron impact ionization source (S_e) for pressures of 25, 50, 75, 100 and 150 mTorr ($\text{Ar}/\text{CF}_4 = 90/10$, $P_{\text{HF}} = P_{\text{LF}} = 300$ W, HF = 150 MHz, LF = 10 MHz). (a) Total power deposition as a function of radius at the HF sheath, (b) total power deposition as a function of height at $r = 5$ cm, (c) S_e as a function of height at $r = 5$ cm and (d) S_e as a function of radius in the HF sheath. The total power deposition and S_e increasingly peak at the HF sheath and in the center of the reactor with increasing pressure.

the dissociative attachment cross sections is also depressed. This effect is most pronounced at higher pressures due to the more distinct separation of the EEDs between the sheath and bulk regions.

The shift in the maximum electron density toward the center of the reactor with increasing pressure observed at a HF of 150 MHz is a function of the HF. For example, at HF = 50 MHz (for otherwise the same operating conditions), the electron density remains edge peaked from 25 mTorr to 150 mTorr. The shortening of the energy relaxation distance with increasing pressure does result in increasing power deposition along the HF sheath. However, different from 150 MHz, the HF electric field is edge peaked at HF = 50 Hz and so is the ionization source. Since the [e] is already edge peaked at 25 mTorr, further increasing the pressure only reinforces this spatial non-uniformity since the power deposition becomes more localized.

The spatial distributions of ions and their fluxes to the wafer ultimately depend on their sources due to electron impact ionization, and their subsequent transport and reactions. The ionization cross sections of Ar and CF₄ (branching to CF₃⁺ and F) have similar thresholds and magnitudes (within a factor of 1.5). However, unlike CF₃⁺, Ar⁺ has large cross sections for symmetric charge exchange and for charge exchange reactions with CF₄ and its fragments [13]. In spite of the larger mass of CF₃, it has a larger effective mobility than Ar⁺ due to the latter's large rate of momentum transfer and depleting reactions. Even though their electron impact source functions are similar, differences between the spatial distributions of Ar⁺ and CF₃⁺ develop with increasing pressure.

For example, the Ar⁺ density and Ar⁺ flux incident on the wafer are shown in figure 7 for pressures of 25, 50, 75 and 100 mTorr for an Ar/CF₄ = 90/10 mixture. With increasing pressure, the maximum [Ar⁺] increases from $1.0 \times 10^{11} \text{ cm}^{-3}$ at 25 mTorr to $2.1 \times 10^{11} \text{ cm}^{-3}$ at 100 mTorr. The spatial distribution of [Ar⁺] follows that of the electron density, shifting toward the center of the reactor and toward the HF electrode. The mean free path for loss of Ar⁺ from charge exchange reactions with CF₄ and its fragments decreases with increasing pressure and so its distribution appears less diffusion dominated and more like its source function. The mean free path for Ar⁺ charge exchanging with CF₄ decreases from about 4 cm at 25 mTorr to 0.8 cm at 150 mTorr [13]. As the source of Ar⁺ moves away from the wafer with increasing pressure and Ar⁺ is depleted by charge exchange reactions while diffusing to the wafer, the Ar⁺ flux to the wafer decreases with increasing pressure.

The CF₃⁺ density and flux incident on the wafer are shown in figure 8. The maximum [CF₃⁺] increases from $4.6 \times 10^{10} \text{ cm}^{-3}$ at 25 mTorr to $2.1 \times 10^{11} \text{ cm}^{-3}$ at 100 mTorr. Although the source of CF₃⁺ undergoes the same transition as that of Ar⁺ with increasing pressure (increasingly center peaked along the HF sheath), the profile of CF₃⁺ is more diffusion dominated. In the absence of significant identity changing charge exchange reactions, volumetric losses are dominated by positive-negative ion recombination. As such, the CF₃⁺ flux incident on the wafer linearly increases with pressure, which reflects the increase in the ionization sources of both Ar⁺ and CF₃⁺.

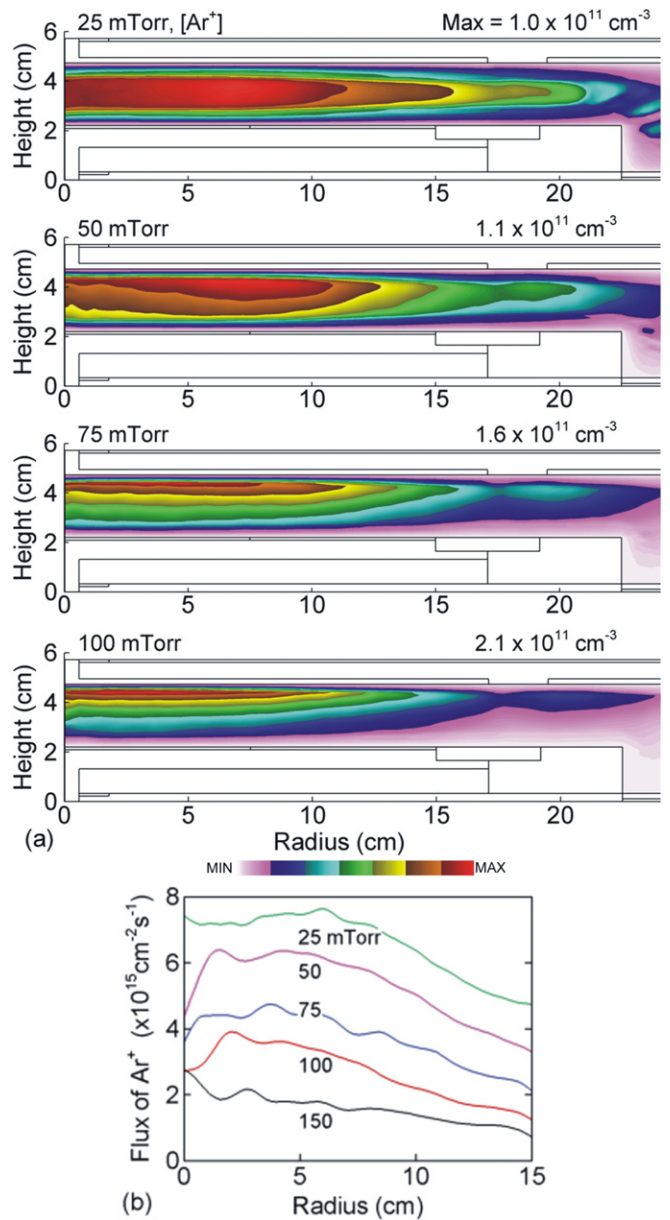


Figure 7. Time averaged Ar⁺ density and flux incident on the wafer for increasing pressure (Ar/CF₄ = 90/10, $P_{\text{HF}} = P_{\text{LF}} = 300 \text{ W}$, HF = 150 MHz, LF = 10 MHz). (a) Ar⁺ density for pressures of 10, 50, 75 and 100 mTorr, (b) Ar⁺ flux onto the wafer. The maximum value or range of values in each frame is noted.

The plasma density at the edge of the lower sheath, and the magnitudes of the LF and HF components in the lower sheath, ultimately determines the radial uniformity of IEADs onto the wafer. To show these dependences, we separately collected IEADs over the center of the wafer (from $r = 0$ to 7.5 cm) and over the edge of the wafer (from $r = 7.5$ to 15 cm). The IEADs for Ar⁺ and CF₃⁺ are shown in figure 9 for pressures of 25 and 150 mTorr. The IEADs for CF₃⁺ are less extended in energy than those for Ar⁺ as CF₃⁺ is heavier and experiences more rf cycles (both HF and LF) when traversing the LF sheath. As the overall uniformity of the plasma is not significantly improved from 25 to 150 mTorr, large center-to-edge ratios of the sheath thickness and the electric field at the lower sheath persist with increasing pressure. Consequently,

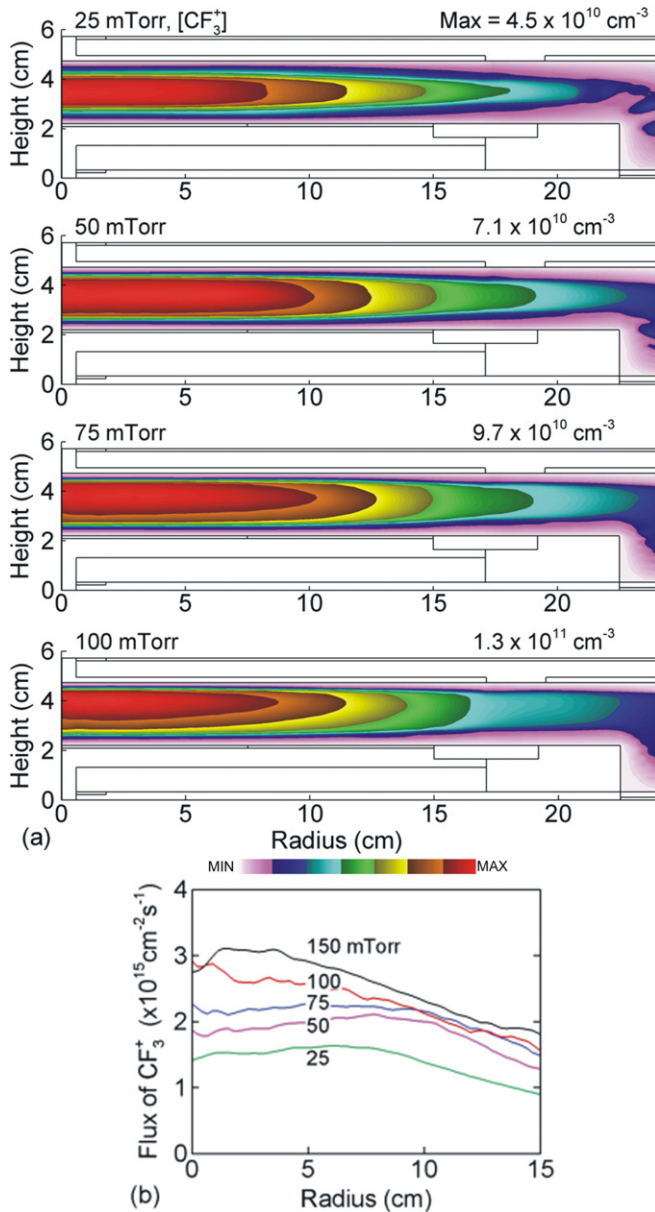


Figure 8. Time averaged CF_3^+ density and flux incident on the wafer for increasing pressure ($\text{Ar}/\text{CF}_4 = 90/10$, $P_{\text{HF}} = P_{\text{LF}} = 300$ W, $\text{HF} = 150$ MHz, $\text{LF} = 10$ MHz). (a) CF_3^+ density for pressures of 10, 50, 75 and 100 mTorr, (b) CF_3^+ flux onto the wafer. The maximum value or range of values in each frame is noted.

there is a large center-to-edge variation of IEADs across the wafer from 25 to 150 mTorr.

3.2. HF power deposition

In an ideal DF-CCP reactor, varying the HF power while keeping other operating conditions unchanged should only modulate the magnitude of the plasma density and leave the spatial distribution of the plasma and the IEADs incident on the wafer unchanged. Booth *et al* experimentally investigated the dependence of electron density and ion flux on rf power in a DF-CCP reactor ($\text{LF} = 2$ MHz and $\text{HF} = 27$ MHz) [14]. They found that both the LF and HF powers have significant effects on the plasma density and the ion flux, in part due to the

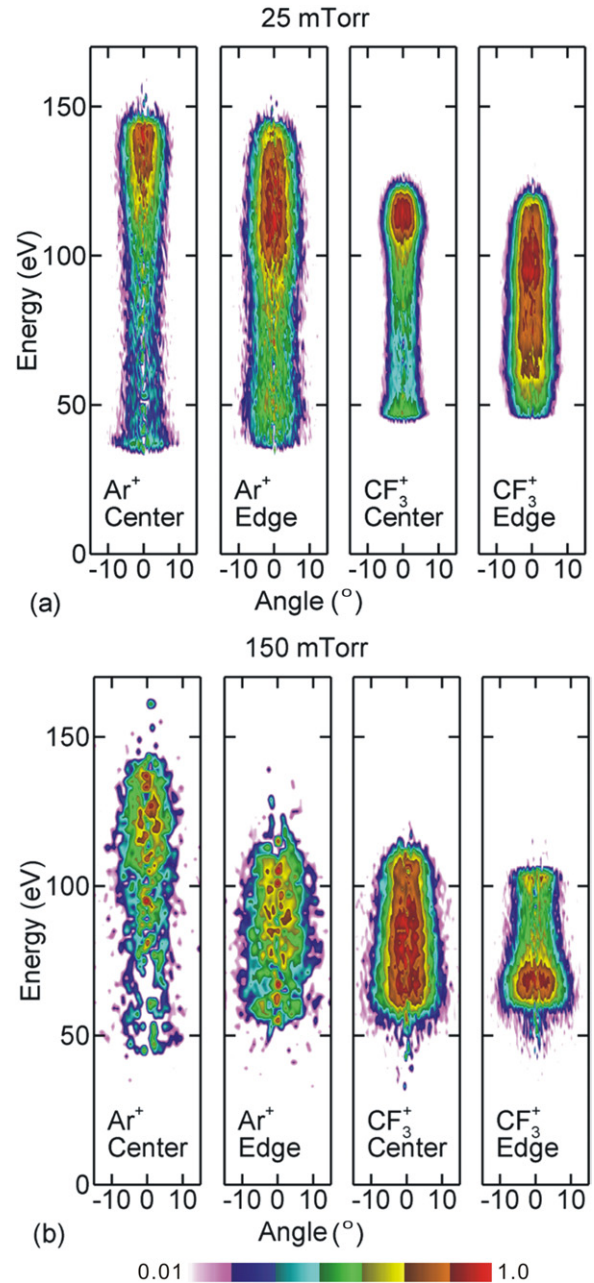


Figure 9. IEADs of Ar^+ and CF_3^+ incident onto the wafer ($\text{Ar}/\text{CF}_4 = 90/10$, $P_{\text{HF}} = P_{\text{LF}} = 300$ W, $\text{HF} = 150$ MHz, $\text{LF} = 10$ MHz). (a) 25 mTorr and (b) 100 mTorr. The IEADs are separately collected over the center of the wafer (from $r = 0$ to $r = 7.5$ cm) and over the edge of the wafer (from $r = 7.5$ to $r = 15$ cm). The IEADs have units of $\text{eV}^{-1} \text{sr}^{-1}$. The contours span two decades using a log scale.

relative small separation between the LF and the HF. The goal of separately controlling the radical fluxes and the ion energies onto the wafer is achieved to some degree in our model reactor when keeping the LF (10 MHz) power constant at 300 W in an $\text{Ar}/\text{CF}_4 = 90/10$ mixture at 50 mTorr. For example, the total negative ion density remains center peaked while varying HF (150 MHz) power deposition (P_{HF}) from 300 to 1000 W, as shown in figure 10(a). The magnitude of the negative ion density increases (and perhaps becomes slightly more center peaked) with power deposition. This is due to the decrease

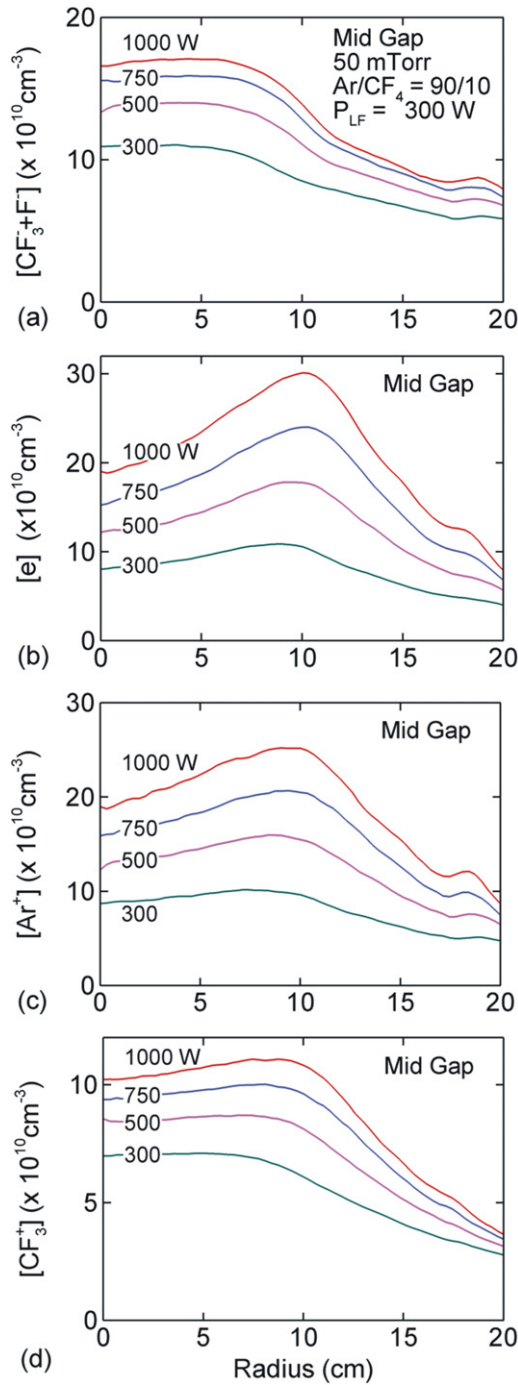


Figure 10. Time averaged plasma densities as a function of radius at the mid-gap for $P_{\text{HF}} = 300, 500, 750$ and 1000 W ($\text{Ar}/\text{CF}_4 = 90/10$, $P_{\text{LF}} = 300$ W, $\text{HF} = 150$ MHz, $\text{LF} = 10$ MHz, 50 mTorr). (a) Total negative ion density ($[\text{CF}_3^- + \text{F}^-]$), (b) electron density, (c) Ar^+ density and (d) CF_3^+ density. The plasma non-uniformity increases with increasing HF power deposition.

in the plasma wavelength with increase in conductivity at higher powers which intensifies the constructive interference at the center of the reactor, though this is a small effect.

The electron density is shown in figure 10(b) while varying P_{HF} from 300 to 1000 W. The maximum electron density nearly linearly increases with P_{HF} , from $1.1 \times 10^{11} \text{ cm}^{-3}$ at 300 W

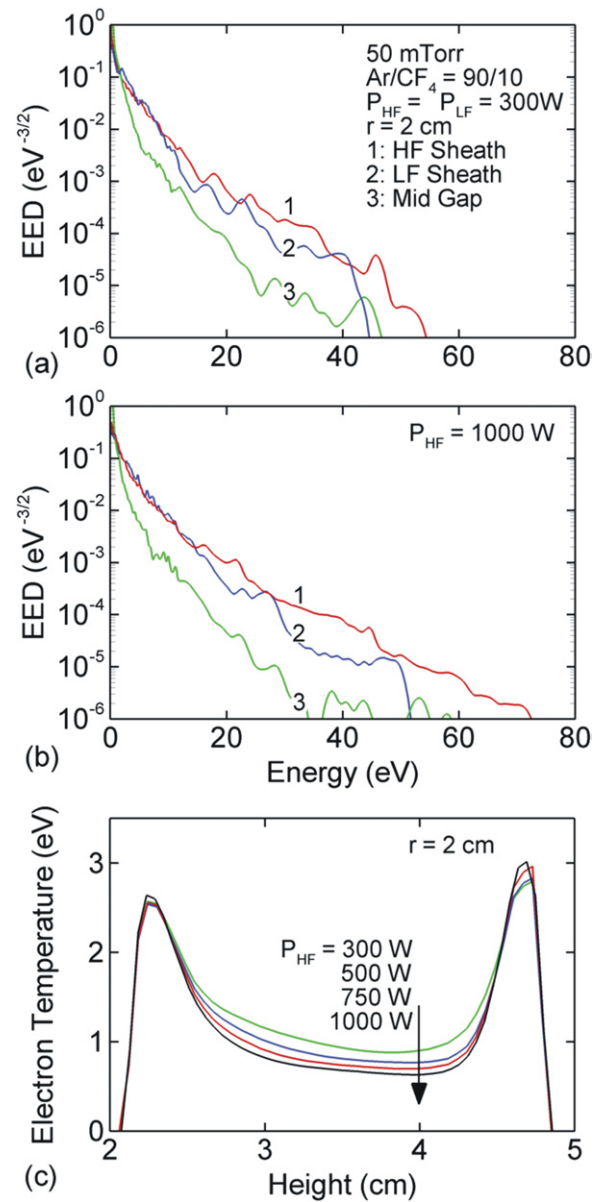


Figure 11. Heating of electrons with increasing P_{HF} ($\text{Ar}/\text{CF}_4 = 90/10$, $P_{\text{LF}} = 300$ W, $\text{HF} = 150$ MHz, $\text{LF} = 10$ MHz, 50 mTorr). (a) EEDs at different axial locations at $r = 2$ cm for $P_{\text{HF}} = 300$ W and (b) $P_{\text{HF}} = 1000$ W, (c) T_e as a function height at $r = 2$ cm. The relative contribution of bulk Ohmic electron heating reduces with increasing P_{HF} due to the increasing electron density.

to $3.0 \times 10^{11} \text{ cm}^{-3}$ at 1000 W. As P_{HF} increases, the electron density profile becomes increasingly mid-radius peaked. This trend results from the combination of at least two factors. First, as P_{HF} increases and excited state densities increase, multi-step ionization processes account for a larger fraction of the total ionization. Since this contribution scales with the square of the electron density, there is a larger fractional change at higher plasma densities. Second, increasing P_{HF} is most efficient at lifting the tails of EEDs near the HF sheath. In the bulk plasma, the EEDs are less affected due to the decreasing skin depth of the HF with increasing electron density, as shown in figures 11(a) and (b). In fact, with increasing P_{HF} Ohmic

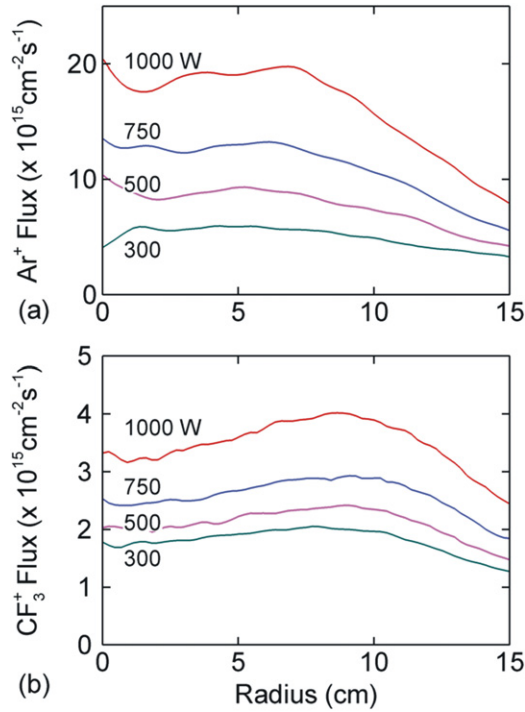


Figure 12. Time averaged ion fluxes incident on the wafer for P_{HF} of 300, 500, 750 and 1000 W ($\text{Ar}/\text{CF}_4 = 90/10$, $P_{\text{LF}} = 300$ W, $\text{HF} = 150$ MHz, $\text{LF} = 10$ MHz, 50 mTorr). (a) Ar^+ flux and (b) CF_3^+ flux.

heating in the bulk plasmas decreases as a fraction of the total power. As a result, the electron temperature T_e ($\langle \varepsilon \rangle = \frac{3}{2}kT_e$) near the HF sheath increases with increasing P_{HF} while T_e in the bulk plasma decreases, as shown in figure 11(c). As a consequence, electron losses from dissociative attachment in the center of the reactor dominate over the gains from ionization (at least, over the range of P_{HF} studied). This trend prevents the maximum of the electron density from moving toward the center of the reactor.

Although the electron density is middle peaked for $P_{\text{HF}} = 300$ –1000 W, the tails of EEDs are most lifted in the center of the reactor. This is a consequence of the maximum in the electric field in the sheath produced by the constructive interference in the finite wavelength effect. The end result is that the $[\text{Ar}^+]$ and $[\text{CF}_3^+]$ profiles, although middle peaked, gain density in the center of the reactor compared with the electron density (figures 10(c) and (d)). The differences between the electron and positive ion densities are attributable to increasing negative ion densities in the center of the reactor due to the (relative) decrease in T_e in the bulk plasma. Due to the lack of charge exchange losses, the $[\text{CF}_3^+]$ profiles are more axially uniform and diffusion dominated compared with those for $[\text{Ar}^+]$.

The radial profiles of ion fluxes incident onto the wafer largely mirror the radial profiles of their densities, and the center-to-edge ratios increase with increasing P_{HF} , as shown in figure 12. The IEADs incident on the wafer, as shown in figure 13, are not independent of P_{HF} for our operating conditions. As the electron and ion densities increase with increasing P_{HF} , the LF voltage decreases to keep the LF power

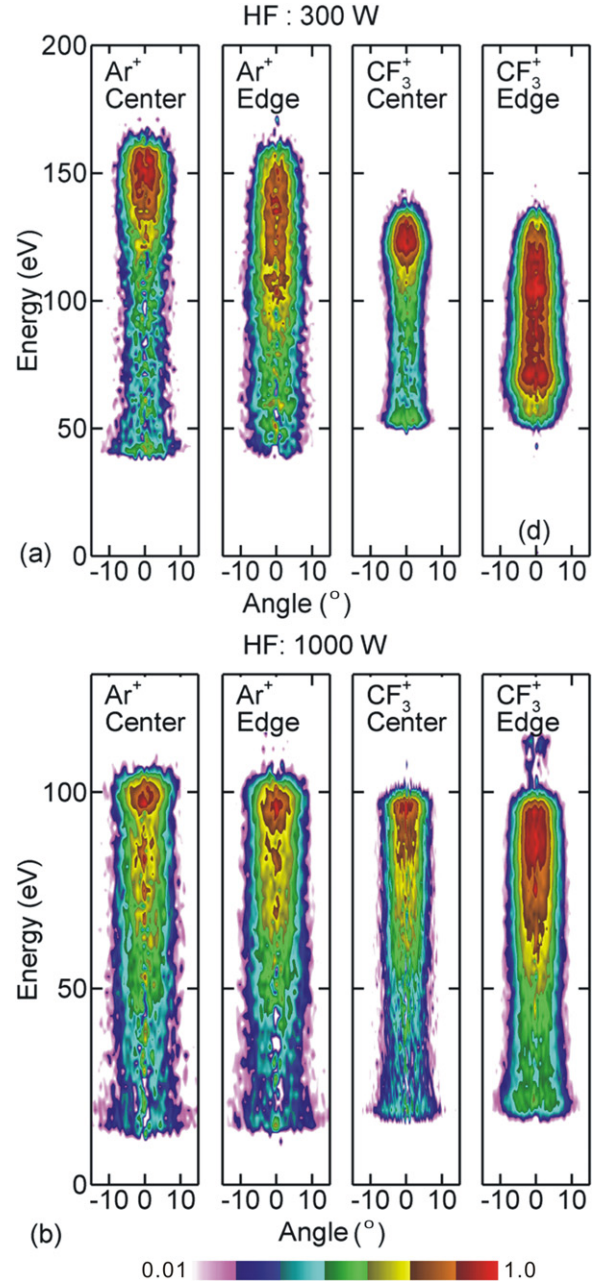


Figure 13. IEADs of Ar^+ and CF_3^+ incident onto the wafer ($\text{Ar}/\text{CF}_4 = 90/10$, $P_{\text{LF}} = 300$ W, $\text{HF} = 150$ MHz, $\text{LF} = 10$ MHz, 50 mTorr). (a) $P_{\text{HF}} = 300$ W and (b) $P_{\text{HF}} = 1000$ W. The IEADs are separately collected over the center of the wafer (from $r = 0$ to $r = 7.5$ cm) and over the edge of the wafer (from $r = 7.5$ to $r = 15$ cm). The IEADs have units of $\text{eV}^{-1} \text{sr}^{-1}$. The contours span two decades using a log scale.

deposition constant. The decrease in LF voltage amplitude for $P_{\text{HF}} = 300$ –1000 W is 160 to 90 V and the change in dc bias is -41 to -5 V. The IEADs therefore degrade in energy and the radial variation is somewhat diminished.

3.3. LF power deposition

In a DF-CCP reactor, the role of the LF power deposition (P_{LF}) is to control the IEADs incident onto the wafer without, ideally, affecting the magnitude of the fluxes nor their spatial

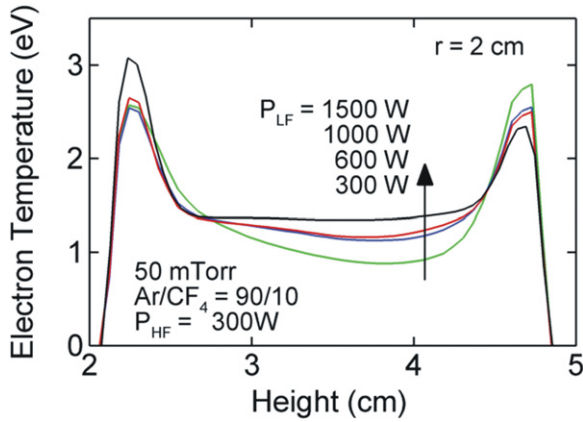


Figure 14. Electron temperature (T_e) as a function of height at $r = 2$ cm for $P_{LF} = 300, 600, 1000$ and 1500 W (Ar/CF₄ = 90/10, $P_{HF} = 300$ W, HF = 150 MHz, LF = 10 MHz, 50 mTorr). Increasing P_{LF} powers mainly increases bulk T_e .

dependences. T_e as a function of height is shown in figure 14 at $r = 2$ cm while varying P_{LF} from 300 to 1500 W. The increase in LF rf amplitude is 160 to 376 V and the change in dc bias is -41 to -110 V. P_{HF} is kept constant at 300 W and the gas mixture is Ar/CF₄ = 90/10 at 50 mTorr. Increasing P_{LF} mainly increases Ohmic heating in the bulk plasma with only a small contribution to stochastic heating due to the increase in sheath speed with increasing amplitude. The bulk T_e therefore increases by only about 0.5 eV (from 0.8 to 1.3 eV at mid-gap in the center of the reactor) for P_{LF} of 300 to 1500 W, though there is a measurable effect.

As a consequence of the small increase in T_e in the bulk plasma with increasing P_{LF} , the rates of attachment decrease while those for ionization increase. For example, at $P_{LF} = 300$ W, there are net losses of electrons in the bulk plasma over the inner two thirds of the wafer due to dissociative attachment [7]. Increasing P_{LF} increases the rate of bulk ionization and the region with net electron losses shrinks. This trend is shown in figure 15, where the electron impact ionization sources by bulk electrons (S_e) and beam electrons (S_{eb}) are shown for P_{LF} of 300 and 1500 W. The region of net negative S_e decreases in volume with increasing P_{LF} , particularly near the center of the reactor. S_{eb} also generally increases with increasing P_{LF} due to the increase in ion fluxes to the wafer which increases the rate of secondary electron emission. Since these secondary electrons are launched into the bulk plasma with nearly the instantaneous LF sheath potential (with increases with P_{LF}) with energies usually exceeding hundreds of eV, they do not directly contribute to the resonant attachment processes as there is little overlap with the cross sections. The increase in ionization rate coefficients are also nominal since the peak in the ionization cross sections occurs at lower energies (about 100 eV) compared with the peak in the secondary electron energies (hundreds of electronvolts). The increase in S_{eb} is largely due to the increase in ion flux.

Following the transition in S_e at the center of the reactor with increasing P_{LF} from being net negative to net positive, the maximum in electron density also shifts inward, as shown in figure 16(a). The maximum electron density increases from $1.1 \times 10^{11} \text{ cm}^{-3}$ for $P_{LF} = 300$ W to $2.4 \times 10^{11} \text{ cm}^{-3}$

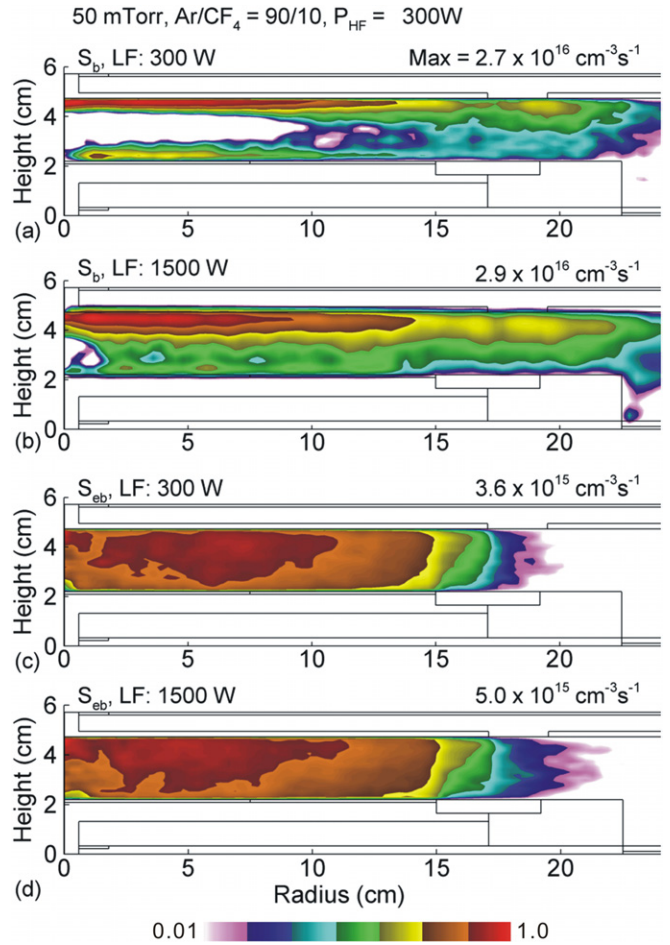


Figure 15. Time averaged ionization source (Ar/CF₄ = 90/10, $P_{HF} = 300$ W, HF = 150 MHz, LF = 10 MHz, 50 mTorr). (a) Net positive ionization sources from bulk electrons (S_e) for $P_{LF} = 300$ W and (b) $P_{LF} = 1500$ W; (c) beam electron ionization source (S_{eb}) for $P_{LF} = 300$ W and (d) $P_{LF} = 1500$ W. The maximum value in each frame is noted. S_e and S_{eb} are plotted on log scales over two decades. In the white region in the center of the reactor the S_e is negative.

at 1500 W, though not in direct proportion to the increase in P_{LF} . This is a consequence of the majority of P_{LF} still being dissipated by ion acceleration. These trends are essentially the same as those measured experimentally, albeit with different operating conditions [14]. The maximum positive ion densities also increases with P_{LF} , though not in direct proportion. The maximum [Ar⁺] at mid-gap increases from $1.0 \times 10^{11} \text{ cm}^{-3}$ at $P_{LF} = 300$ W to $1.7 \times 10^{11} \text{ cm}^{-3}$ at 1500 W. The positive ion densities also transition from being middle peaked to center peaked as P_{LF} increases, as shown in figures 16(b) and (d). The maximum negative ion density at mid-gap decreases from $1.1 \times 10^{11} \text{ cm}^{-3}$ at $P_{LF} = 300$ W to $8.8 \times 10^{10} \text{ cm}^{-3}$ at 1500 W. This small decrease likely results from the increase in T_e in the bulk plasma which is not necessarily favorable to attachment processes. With the increase in electron density, the shift toward the center of the reactor is exacerbated by the finite wavelength effect. The higher plasma density produces a shorter wavelength which contributes to more intense constructive interference in the center of the reactor.

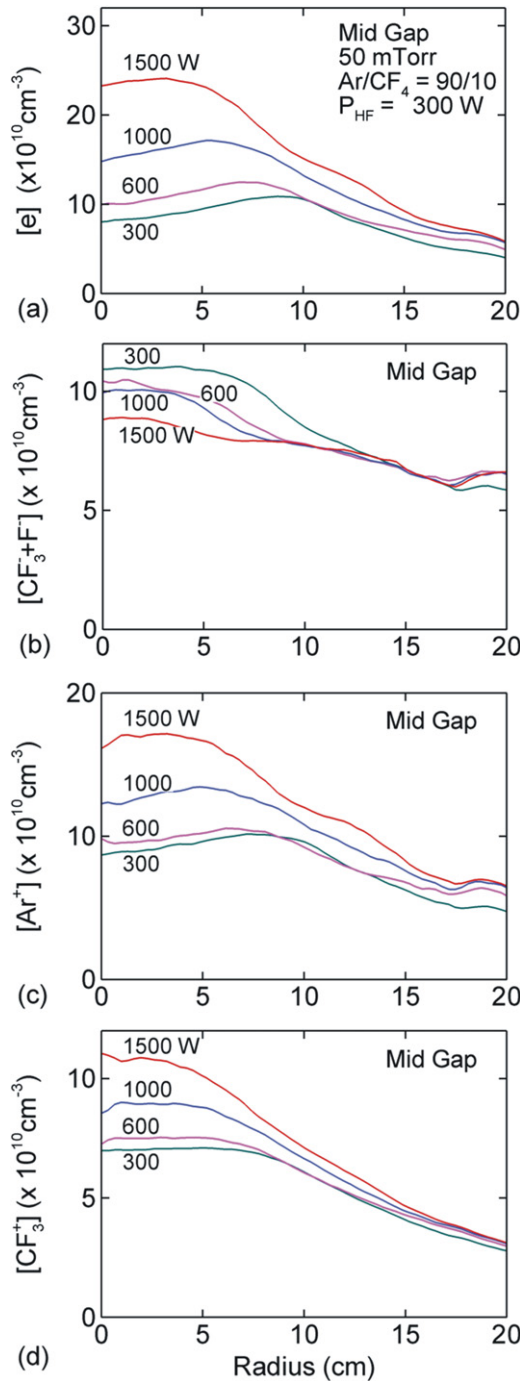


Figure 16. Time averaged plasma densities as a function of radius at the mid-gap for $P_{LF} = 300, 600, 1000$ and 1500 W ($Ar/CF_4 = 90/10, P_{HF} = 300$ W, $HF = 150$ MHz, $LF = 10$ MHz, 50 mTorr). (a) Electron density, (b) total negative ion density ($[CF_3^- + F^-]$), (c) Ar^+ density and (d) CF_3^+ density. The plasma non-uniformity increases with increasing LF power deposition.

In the model reactor, the magnitude of the ion fluxes, the ion energies onto the wafer and their spatial dependences are functions of P_{LF} . The fluxes of positive ions largely mirror their respective ion densities, transitioning from being middle peaked to being center peaked with increasing P_{LF} , as shown in figure 17. As the LF rf amplitude increases with P_{LF} to deposit more power, the IEADs incident on the wafer shift up in energy and also narrow in angle. For example, the IEADs incident

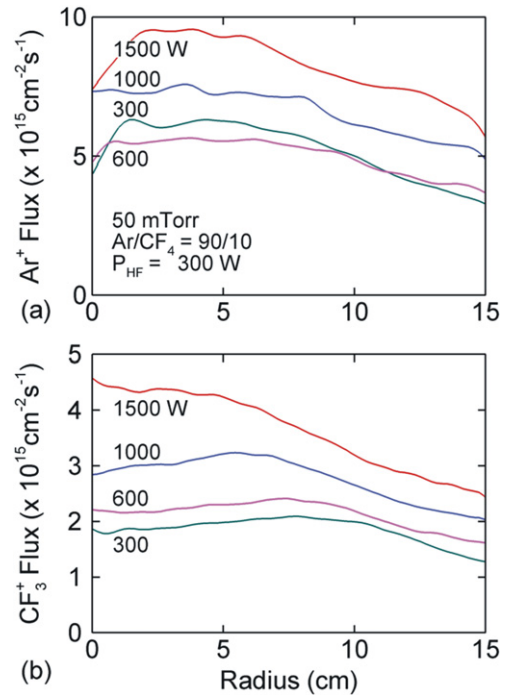


Figure 17. Ion fluxes incident on the wafer for LF power of $300, 600, 1000$ and 1500 W ($Ar/CF_4 = 90/10, P_{HF} = 300$ W, $HF = 150$ MHz, $LF = 10$ MHz, 50 mTorr). (a) Ar^+ flux and (b) CF_3^+ flux.

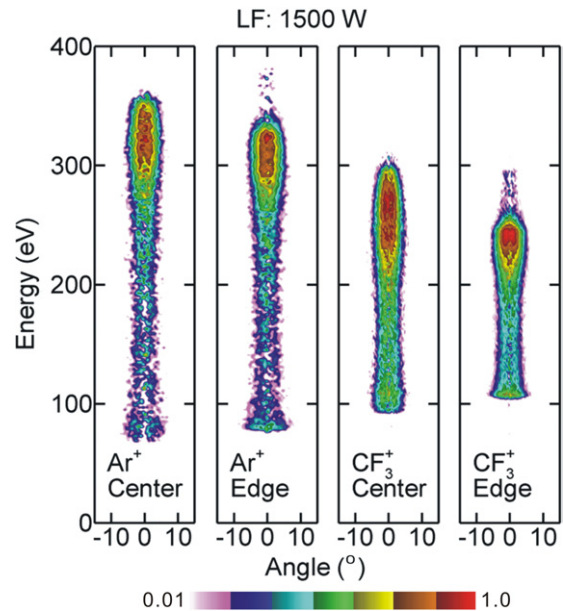


Figure 18. IEADs of Ar^+ and CF_3^+ incident onto the wafer for $P_{LF} = 1500$ W ($Ar/CF_4 = 90/10, P_{HF} = 300$ W, $HF = 150$ MHz, $LF = 10$ MHz, 50 mTorr). The IEADs are separately collected over the center of the wafer (from $r = 0$ to $r = 7.5$ cm) and over the edge of the wafer (from $r = 7.5$ to $r = 15$ cm). The IEADs have units of $eV^{-1} sr^{-1}$. The contours span two decades using a log scale.

onto the wafer for $P_{LF} = 1500$ W are shown in figure 18. (See figure 13(a) for IEADs with $P_{LF} = 300$ W.) This is, to some degree, the desired result—controlling the shape of the IEAD with LF power if other plasma properties, such as magnitude and uniformity of fluxes, are not affected. As the

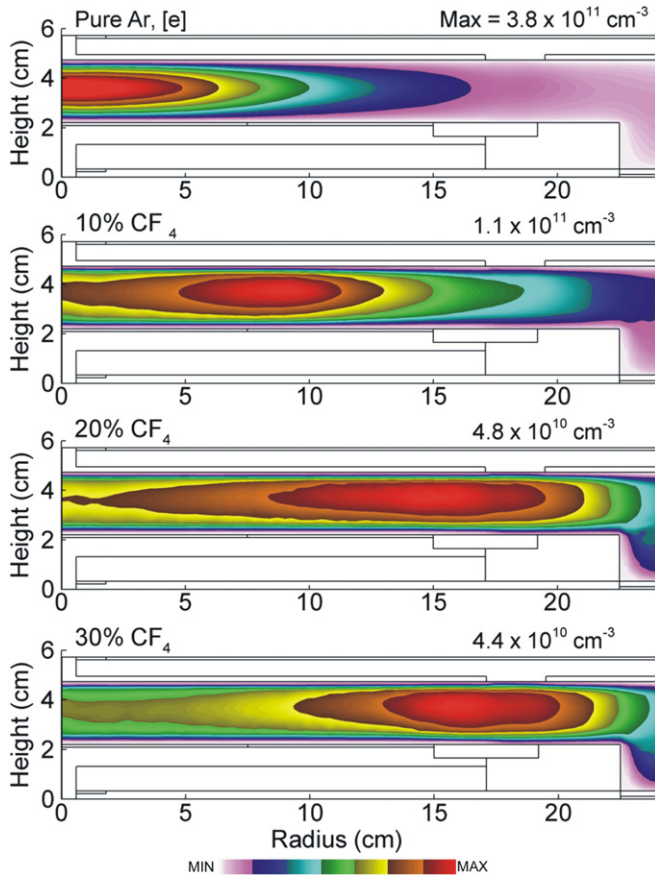


Figure 19. Time averaged electron density (e) for CF_4 fractions of 0, 0.1, 0.2 and 0.3 in argon ($P_{\text{HF}} = P_{\text{LF}} = 300$ W, $\text{HF} = 150$ MHz, $\text{LF} = 10$ MHz, 50 mTorr). The maximum value in each frame is noted. The maximum of the electron density shifts toward the edge of the electrode with increasing CF_4 fraction due, in part, to the increasing effective plasma wavelength making the system appear more ES.

plasma remains non-uniform with increasing P_{LF} , so do the LF sheath thickness and the electric field at the lower electrode. Hence a large center-to-edge variation of IEADs across the wafer persist with increasing P_{LF} from 300 to 1500 W.

3.4. Gas chemistry

In HF CCPs, the relative importance of EM and ES effects are functions of the gas mixture, particularly with electronegative mixtures, through its influence on the conductivity of the plasma. This in turn impacts the uniformity of the plasma. For example, Rauf *et al* investigated the consequences fractional substitution of CF_4 and SF_6 to 100 mTorr of argon in a 100 W CCP operating at 180 MHz [15]. They found that the maximum of the electron density shifted toward the edges of the electrodes with increasing SF_6 and CF_4 fraction, effects attributed to the change in spatial dependence of conductivity with addition of the electronegative gases. The outward shift in electron density in Ar/CF_4 was less intense due to the lower electronegativity of CF_4 compared with SF_6 .

Our results for scaling of plasma properties with CF_4 fraction in Ar/CF_4 mixtures generally agree with those of Rauf *et al* [15]. For example, the electron density is shown

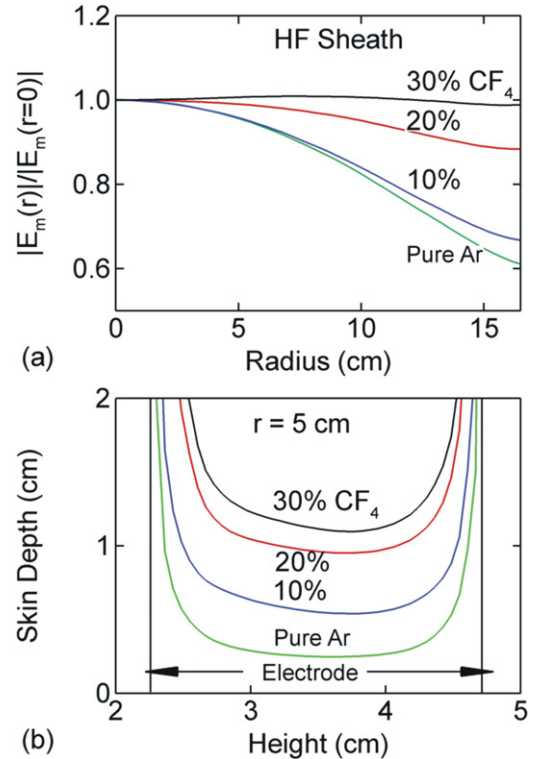


Figure 20. EM properties for CF_4 fractions of 0, 0.1, 0.2 and 0.3 in argon ($P_{\text{HF}} = P_{\text{LF}} = 300$ W, $\text{HF} = 150$ MHz, $\text{LF} = 10$ MHz, 50 mTorr). (a) Magnitude of the HF electric field (first harmonic amplitude, $|E_m(r)|$) along the HF sheath (normalized by the magnitude of the field at the center of the reactor) and (b) skin depth as a function of height at $r = 5$ cm.

in figure 19 for CF_4 fractions of 0 to 0.3 at pressure of 50 mTorr and $P_{\text{LF}} = P_{\text{HF}} = 300$ W. With increasing CF_4 fraction there is a systematic shift of the peak electron density toward the edge of the electrodes and a decrease in the peak electron density (from $3.8 \times 10^{11} \text{ cm}^{-3}$ for pure Ar to $4.4 \times 10^{10} \text{ cm}^{-3}$ for $\text{Ar}/\text{CF}_4 = 70/30$). As the electron density decreases, so does the conductivity of the plasma. The effective plasma wavelength therefore increases which weakens the finite wavelength effect by reducing constructive interference at the center of the electrode. This weakening is shown in figure 20(a), where the electric field along the HF sheath is plotted as a function of radius. With increasing CF_4 fraction, the electric field in the HF sheath becomes less center peaked and the plasma becomes more ES in nature [15]. Another consequence of the decreasing electron density is an increase in the skin depth, as shown in figure 20(b), which contributes to more bulk electron heating and so improves the overall uniformity of the plasma.

As the uniformity of the electron density improves with increasing CF_4 fraction, the radial uniformities of ion densities and their fluxes incident on the wafer also improve, as shown in figures 21 and 22. The axial gradient for $[\text{Ar}^+]$ is more severe compared with $[\text{CF}_3^+]$ due to the larger rate of charge exchange reactions which deplete Ar^+ [13]. The density and flux of Ar^+ decrease, while those of CF_3^+ increase, with increasing CF_4 fraction. The uniformities of the plasma and fluxes to the wafer optimize at a CF_4 fraction of about 0.2.

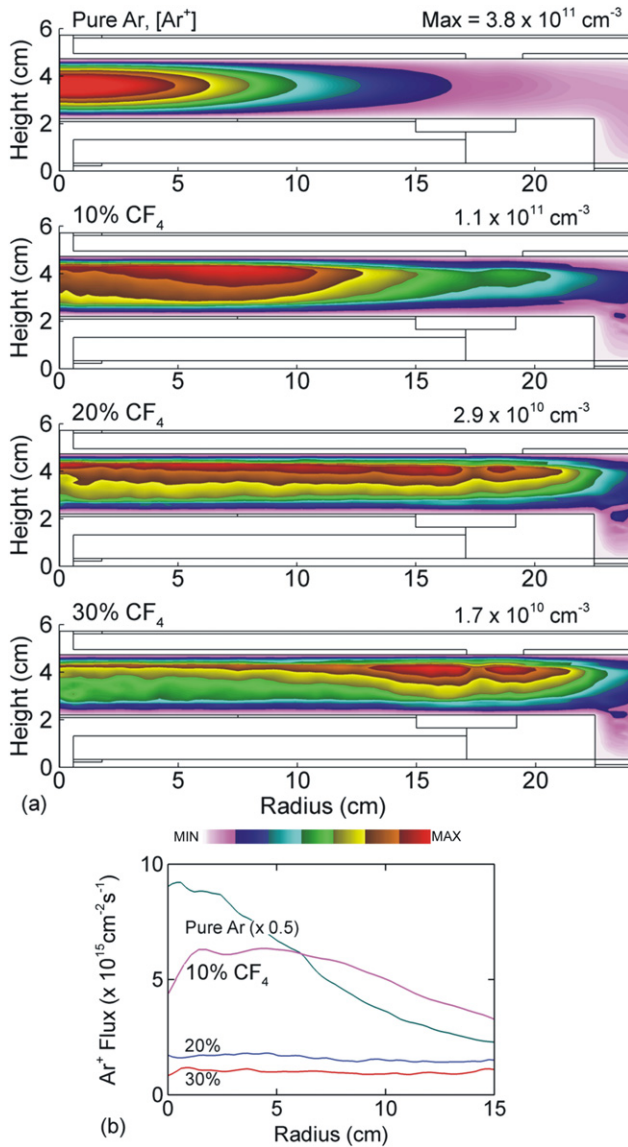


Figure 21. Time averaged Ar^+ density and flux incident on the wafer for CF_4 fractions of 0, 0.1, 0.2 and 0.3 in argon ($P_{\text{HF}} = P_{\text{LF}} = 300 \text{ W}$, $\text{HF} = 150 \text{ MHz}$, $\text{LF} = 10 \text{ MHz}$, 50 mTorr). (a) Ar^+ density and (b) Ar^+ flux onto the wafer. The maximum value or range of values in each frame is noted.

As the uniformity of the thickness and the magnitude of the electric field in the LF sheath track that of the plasma, the uniformity of the IEADs to the wafer are also functions of the CF_4 fraction. For example, IEADs incident to the wafer for Ar^+ and CF_3^+ are shown in figure 23 for $\text{Ar}/\text{CF}_4 = 0.8/0.2$. Due to the improved uniformity of the plasmas, the center-to-edge uniformity of IEADs also improves compared with lower CF_4 fractions. (See figure 13(a) for IEADs with $\text{Ar}/\text{CF}_4 = 90/10$.)

4. Concluding remarks

The consequences of pressure, LF and HF power deposition, and gas mixtures on plasma uniformity in a DF-CCP reactor sustained in Ar/CF_4 mixtures have been computationally investigated using results from a two-dimensional plasma transport model. A full-wave Maxwell solver was developed

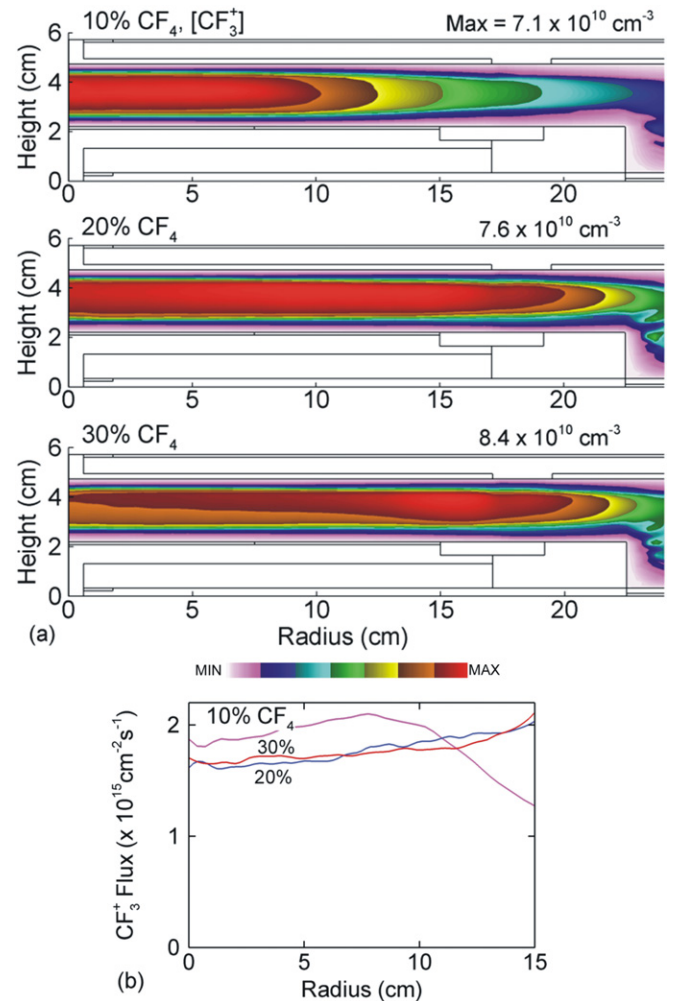


Figure 22. Time averaged CF_3^+ density and flux incident on the wafer for CF_4 fractions of 0, 0.1, 0.2 and 0.3 in argon ($P_{\text{HF}} = P_{\text{LF}} = 300 \text{ W}$, $\text{HF} = 150 \text{ MHz}$, $\text{LF} = 10 \text{ MHz}$, 50 mTorr). (a) CF_3^+ density and (b) CF_3^+ flux onto the wafer. The maximum value or range of values in each frame is noted. The CF_3^+ density is plotted on a linear scale.

and integrated into the model to resolve EM and ES effects. With increasing pressure, while keeping other operating conditions unchanged ($P_{\text{HF}} = P_{\text{LF}} = 300 \text{ W}$, 50 mTorr , $\text{Ar}/\text{CF}_4 = 90/10$), the maximum of the electron density shifts toward the center of the reactor and toward the HF electrode. The shift toward the HF electrode is due to the decreasing energy relaxation distance with increasing pressure. As more power is dissipated closer to the HF sheath, the bulk electron ionization source increasingly mirrors the electric field in the HF sheath which is center peaked due to the finite wavelength effect. Changes in power deposition due to changes in skin depth and inductive heating are not major effects for our operating conditions.

With increasing P_{HF} ($P_{\text{LF}} = 300 \text{ W}$, 50 mTorr , $\text{Ar}/\text{CF}_4 = 90/10$), the uniformity of the plasma decreases and the electron density becomes increasingly mid-peaked. Though the ionization sources are center peaked along the HF sheath, the large rates of attachment in the bulk plasma at the center of the reactor prevent the peak electron density from moving inward. Increasing P_{HF} also results in a degradation in

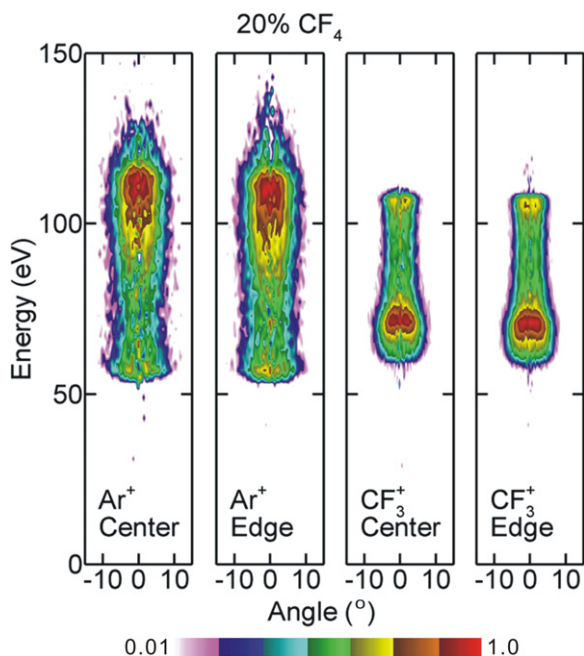


Figure 23. IEADs of Ar^+ and CF_3^+ incident onto the wafer for Ar/CF_4 fraction = 0.8/0.2 ($P_{\text{HF}} = P_{\text{LF}} = 300$ W, $\text{HF} = 150$ MHz, $\text{LF} = 10$ MHz, 50 mTorr). The IEADs are separately collected over the center of the wafer (from $r = 0$ to $r = 7.5$ cm) and over the edge of the wafer (from $r = 7.5$ to $r = 15$ cm). The IEADs have units of $\text{eV}^{-1} \text{sr}^{-1}$. The contours span two decades using a log scale.

the energy of the IEADs incident on the wafer. The LF voltage decreases with increasing plasma density to maintain a constant LF power deposition.

Increasing P_{LF} ($P_{\text{HF}} = 300$ W, 50 mTorr, $\text{Ar}/\text{CF}_4 = 90/10$) increases bulk and beam ionization and while reducing net electron losses from dissociative attachment processes in the center of the reactor. As a result, the electron density becomes increasingly center peaked. Exceeding $P_{\text{LF}} = 1000$ W, the plasmas become non-uniform and with large center-to-edge variations of ion fluxes and IEADs incident on the wafer.

Increasing the CF_4 fraction ($P_{\text{HF}} = P_{\text{LF}} = 300$ W, 50 mTorr) in argon decreases the electron density thereby increasing the effective plasma wavelength. The uniformity of the electric field along the HF sheath consequently improves thereby improving the uniformity of the plasma. For our conditions, the uniformity of ion fluxes and IEADs incident onto the wafer optimize with CF_4 fractions of about 0.2.

Due to the coupling of finite wavelength, EM skin, ES edge and electronegative effects, there are no simple scaling laws for plasma uniformity when varying gas mixture, power and pressure. The plasma uniformity is a function of conductivity and energy relaxation distance with strong second-order effects due to feedback of EEDs on ionization sources. The consequences of the operating parameters on the plasma properties in DF-CCP reactors can be better understood by analyzing the correlation of finite wavelength, EM skin, ES edge and electronegative effects and their impact on the spatial distributions of EEDs.

Acknowledgment

This work was supported by the Semiconductor Research Corp., Applied Materials Inc., Tokyo Electron Ltd and the US Department of Energy Office of Fusion Energy Sciences.

References

- [1] Bera K, Rauf S, Ramaswamy K and Collins K 2009 *J. Appl. Phys.* **106** 033301
- [2] Gans T, Schulze J, O'Connell D, Czarnetzki U, Faulkner R, Ellingboe A R and Turner M M 2006 *Appl. Phys. Lett.* **89** 261502
- [3] Yagisawa T, Shimada T and Makabe T 2005 *J. Vac. Sci. Technol. B* **23** 2212
- [4] Donko Z and Petrovic Z Lj 2006 *Japan. J. Appl. Phys.* **45** 8151
- [5] Chabert P 2007 *J. Phys. D: Appl. Phys.* **40** R63
- [6] Lieberman M A, Booth J P, Chabert P, Rax J M and Turner M M 2002 *Plasma Sources Sci. Technol.* **11** 283
- [7] Yang Y and Kushner M J 2010 *Plasma Sources Sci. Technol.* **19** 055011
- [8] Kushner M J 2009 *J. Phys. D: Appl. Phys.* **42** 194013
- [9] Rauf S and Kushner M J 1997 *J. Appl. Phys.* **82** 2805
- [10] Hebner G A, Barnat E V, Miller P A, Paterson A M and Holland J P 2006 *Plasma Sources Sci. Technol.* **15** 879
- [11] Volynets V N, Ushakov A G, Sung D, Tolmachev Y N, Pashkovsky V G, Lee J B, Kwon T Y and Jeong K S 2008 *J. Vac. Sci. Technol. A* **26** 406
- [12] Lieberman M A and Lichtenberg A J 2005 *Principles of Plasma Discharges and Materials Processing* (New York: Wiley) p 706
- [13] Fisher E R, Weber M E and Armentrout P B 1990 *J. Chem. Phys.* **92** 2296
- [14] Booth J P, Curley G, Maric D and Chabert P 2010 *Plasma Sources Sci. Technol.* **19** 015005
- [15] Rauf S, Bera K and Collins K 2008 *Plasma Sources Sci. Technol.* **17** 035003